Understanding light scattering by a coated sphere Part 2: Time domain analysis

Philip Laven[1] and James A. Lock[2,*]

[1]*9 Russells Crescent, Horley RH6 7DJ, UK*
[2]*Department of Physics, Cleveland State University, Cleveland, Ohio 44115, USA*
**Corresponding author: j.lock@csuohio.edu*

Received April 9, 2012; revised May 31, 2012; accepted May 31, 2012;
posted May 31, 2012 (Doc. ID 166287); published July 9, 2012

Numerical computations were made of scattering of an incident electromagnetic pulse by a coated sphere that is large compared to the dominant wavelength of the incident light. The scattered intensity was plotted as a function of the scattering angle and delay time of the scattered pulse. For fixed core and coating radii, the Debye series terms that most strongly contribute to the scattered intensity in different regions of scattering angle-delay time space were identified and analyzed. For a fixed overall radius and an increasing core radius, the first-order rainbow was observed to evolve into three separate components. The original component faded away, while the two new components eventually merged together. The behavior of surface waves generated by grazing incidence at the core/coating and coating/exterior interfaces was also examined and discussed.

OCIS codes: 080.5692, 290.4020, 320.2250.

1. INTRODUCTION

In the first part of this study [1], we considered an electromagnetic plane wave traveling in an exterior medium (region 3) of real refractive index m_3, which is scattered by a coated sphere of overall radius a_{23}, and consisting of a core (region 1) of radius a_{12} and real refractive index m_1 concentrically surrounded by a coating (region 2) of real refractive index m_2. The partial wave scattering amplitudes, first derived by Aden and Kerker [2], were expanded in a Debye series [3,4], which was then reorganized in terms of differing total numbers N of internal reflections. These consist of N^{212} of the R_n^{212} internal reflections of a partial wave in region 2 at the core/coating interface back into region 2 again, N^{121} of the R_n^{121} internal reflections of a partial wave in region 1 at the core/coating interface back into region 1 again, and N^{232} of the R_n^{232} internal reflections of a partial wave in region 2 at the coating/exterior interface back into region 2 again, with $N^{212}+N^{121}+N^{232}=N$. The various Debye terms were parameterized by (N,A,B), where the paths of the corresponding light rays through the coated sphere, as obtained using van de Hulst's localization principle [5], have A chords in the coating region and B chords in the core region. Using this parameterization it was found in [1] that all the Debye series terms with the same values of N, A, and B for plane wave incidence have the same scattered field as a function of the scattering angle θ. This is called path degeneracy. In time domain scattering, a short electromagnetic pulse is incident on the coated sphere and the scattered intensity is plotted as a function of θ and the delay time t of the scattered pulse [6–9]. Since the optical path length of the corresponding light rays of each Debye term depends only on A and B as well, these different paths also have the same intensity in $\theta-t$ space for time domain scattering.

In addition, some of the (N,A,B) terms are recurrences of the $(N-2,A,B)$ terms. These are called repeated paths. For these terms the (N,A,B) rays have the same time domain trajectory in $\theta-t$ space as do the rays for $(N-2,A,B)$. But since the $(N-2,A,B)$ Debye term contains extra partial wave transmission coefficients while the (N,A,B) term contains extra partial wave reflection coefficients, the scattered intensity of the (N,A,B) and $(N-2,A,B)$ terms differs along the repeated $\theta-t$ trajectory. Both path degeneracy and the repeated terms greatly reduce the number of Debye terms that need to be examined for a given value of N. For example, there are 353 Debye terms for $N=7$. Taking path degeneracy into account there are only 21 independent Debye terms. If the repeated terms are also taken into account for time domain scattering, there are only 12 new trajectories in $\theta-t$ space that did not occur for $N=5$. These geometrical effects greatly reduce the complexity of the analysis of scattering by a coated sphere.

The body of this paper is organized as follows. In Section 2 we consider scattering by coated sphere with a fixed core radius. We identify the dominant Debye terms for scattering in a number of different regions of $\theta-t$ space, and point out some interesting scattering effects occurring in various terms. In Section 3 we consider scattering for varying core radius. Again we determine the dominant Debye terms, and also study the evolution of both the first-order rainbow and the core/coating surface waves as a function of core size. In Section 4 we present some concluding remarks. All of the results in this paper have been generated using the MiePlot computer program, which can be downloaded free of charge from www.philiplaven.com/mieplot.htm.

2. COATED SPHERE WITH A CORE OF FIXED RADIUS

We first considered a 5 fs temporally Gaussian and spatially plane wave pulse whose Fourier spectrum is centered on $\lambda=0.65$ μm and truncated at –60 dB as described in detail in [8].

The pulse is incident on a coated sphere with core refractive index $m_1 = 1.5$, coating refractive index $m_2 = 1.3333$, and radii $a_{12} = 7.5\ \mu$m, $a_{23} = 10\ \mu$m in an external medium with $m_3 = 1$. In this situation, the core is "particle-like" with respect to the coating since $m_1 > m_2$. If $m_1 < m_2$, the core would have been "bubble-like" with respect to the coating and many details of the scattering would have been quite different. Since $m_2/m_3 = 4/3$ and $a_{12}/a_{23} = 3/4$, a ray tracing analysis as described in [1] shows that an incident light ray grazing the edge of the coating and transmitted into it at the critical angle also has grazing incidence on the core. Physically this means that core/coating and coating/exterior electromagnetic surface waves are generated by the same edge rays and cannot be distinguished from each other when plotted as a function of scattering angle alone.

For each wave number k appearing in the Fourier spectrum of the incident pulse, the transverse electric ($i = 1$) and transverse magnetic ($i = 2$) scattering amplitude is $S_i(\theta)$, where

$$S_1(\theta) = \sum_{n=1}^{\infty}\{(2n+1)/[n(n+1)]\}[a_n\pi_n(\theta) + b_n\tau_n(\theta)] \quad (1a)$$

$$S_2(\theta) = \sum_{n=1}^{\infty}\{(2n+1)/[n(n+1)]\}[a_n\tau_n(\theta) + b_n\pi_n(\theta)], \quad (1b)$$

$\pi_n(\theta)$ and $\tau_n(\theta)$ are the angular functions of Mie theory [10], and a_n and b_n are either the full Aden–Kerker partial wave scattering amplitudes, or those of the specific (N, A, B) Debye term being studied. Since the refractive indices of the core and coating were taken to be real, the spherical Bessel functions appearing in a_n and b_n were calculated using either upward recursion or downward recursion in double precision, depending on the relative values of n_2ka_{12}, n_1ka_{12}, and n_2ka_{23} to the largest partial wave required for convergence of the partial wave sum in Eqs. (1a) and (1b). The scattering amplitude is then multiplied by $F(k)$, the weighting function of the Fourier spectrum of the incident pulse, and the result is then inverse Fourier transformed back to the time domain using the $2^{15} = 32,768$ point fast Fourier transform algorithm. The time domain intensity is proportional to the square of the magnitude of the time domain electric field, which is plotted as a function of the scattering angle and delay time of the scattered pulse as in [6–9].

The intensity obtained from the full Aden–Kerker scattering calculations is shown in false color in Fig. 1, where the time delay of the scattered pulse is measured relative to that of the pulse that is externally reflected at $\theta = 180°$ from the coating/exterior interface. The most important Debye series contributions are labeled by their (N, A, B) value in the figure. The physical meaning of each (N, A, B) Debye term is described in [1], and the identifications in Fig. 1 are based on a comparison with the corresponding time domain ray trajectories. This figure, when compared with Fig. 1 of [8], which shows time domain scattering of a similar incident pulse by a homogeneous sphere of radius 10 μm, illustrates the great richness in structure of scattering by a coated sphere. This structure is much more evident in the time domain, where all the different scattering mechanisms contributing at the same scattering angle are separated by their differing delay times. If the scattered intensity had been plotted solely as a function of θ, all the scattering mechanisms would be superposed and

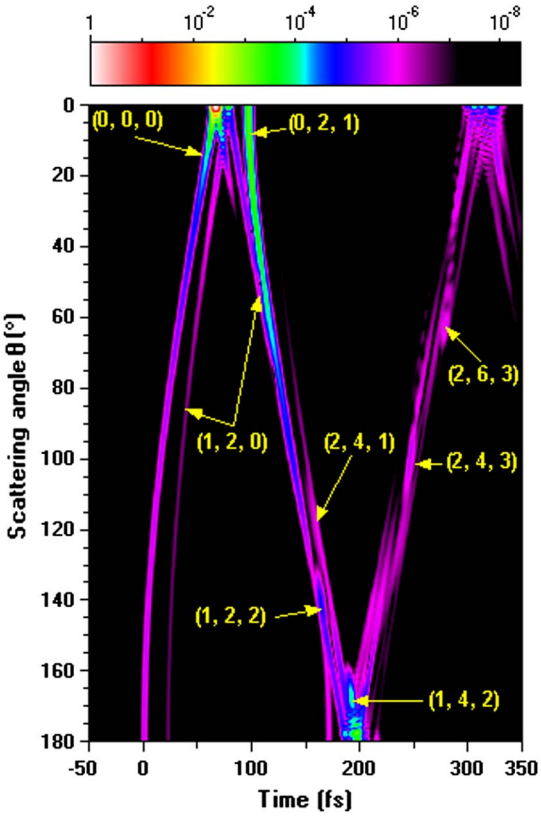

Fig. 1. (Color online) Scattered intensity as a function of the scattering angle θ and delay time t of a 5 fs unpolarized Gaussian pulse by a coated sphere of core radius $a_{12} = 7.5\ \mu$m and refractive index $m_1 = 1.5$, coating refractive index $m_2 = 1.3333$, and overall radius $a_{23} = 10\ \mu$m. The dominant Debye series contributions (N, A, B) in different regions of $\theta - t$ space are indicated.

interfere with each other. The time domain method allows one to examine the weaker contributions in detail without having them obscured by the stronger contributions.

The time domain path of reflection at the coating/core interface (1, 2, 0) is delayed with respect to that of external reflection at the coating/exterior interface (0, 0, 0) due to the two extra passes of the pulse through the coating. The (0, 2, 1) term for direct transmission through both the core and coating is qualitatively similar to its behavior for scattering by a homogeneous sphere of the same overall size [7,8]. As the (0, 2, 1) contribution dies out for larger delay times, the two-fold degenerate contribution of the (2, 4, 1) term, corresponding to transmission through the coated sphere following two successive reflections within the coating, becomes dominant. The first-order rainbow of (1, 4, 2) dominates scattering for $\theta \approx 170°$. The internal reflection for this term occurs at the coating/exterior interface and was called the β rainbow in [4]. The first-order rainbow in (1, 2, 2) is visible at $\theta \approx 142°$. The internal reflection for this term occurs at the core/coating interface and was called the α rainbow in [4]. Since the coating/exterior reflection is stronger than the core/coating reflection, the β rainbow is brighter than the α rainbow. The backscattering region in Fig. 1 is dominated by the (2, 4, 1) and (1, 4, 2) glories. For longer delay times, the (2, 4, 3) and (2, 6, 3) second-order rainbows are dominant. The forward scattering region at $t \approx 300$ fs is dominated by the (2, 6, 3) glory, which makes three complete passes through

the coated sphere with two reflections at the coating/exterior interface, and the (3, 4, 4) third-order rainbow and double glory to be described in more detail below.

Figure 2(a) is a magnified view of Fig. 1 for 130° ≤ θ ≤ 180° and 150 fs ≤ t ≤ 230 fs. In this figure, the α and β twin first-order rainbows due to the (1, 2, 2) and (1, 4, 2) terms are clearly resolved, together with the (2, 4, 1) glory and the barely visible (2, 2, 3) second-order rainbow. The corresponding ray trajectories are overlaid on the figure with grid ticks corresponding to the incident ray impact parameter $b = \sin(\theta_{3i})$ at intervals of $\Delta b = 0.1$. The resolution of the different Debye terms improves further in Fig. 2(b) where we examined scattering of a 5 fs pulse by a substantially larger coated sphere with $a_{12} = 30$ μm and $a_{23} = 40$ μm. A number of weaker scattering processes are now resolved as well. The improvement in the resolution is due to the fact that ray scattering is a better approximation to wave scattering as the particle size increases.

Figure 3 is a magnified view of Fig. 1 for 200 fs ≤ t ≤ 400 fs. This illustrates the increasingly longer delay times of the (2, 2, 3), (2, 4, 3), and (2, 6, 3) Debye terms for near-axial incidence due to 2 or 4 or 6 passes of the corresponding rays through the coating. It also shows the rainbows of these Debye terms at $\theta \approx 142°$, 97° and 63°, which we call the $\alpha\alpha$, $\alpha\beta$, and $\beta\beta$ second-order rainbows, respectively, where, as before, α indicates a core/coating internal reflection and β indicates a coating/exterior internal reflection. The $\alpha\beta$ rainbow consists of the two-fold degenerate contributions of Figs. 2(i) and 2(j) of [1]. The strong scattered intensity at $\theta \approx 0°$ in the interval 300 fs ≤ t ≤ 330 fs is due to the superposition and interference of the surface wave forward glory of the (2, 4, 3) term and the real ray forward glories of the (2, 6, 3) and (3, 4, 4) terms.

As mentioned above, the identifications of the dominant contributions to the Aden–Kerker coated sphere time domain scattering signature were made on he basis of ray scattering predictions. In order to verify these identifications using wave scattering, we computed the unpolarized scattered intensity as a function of θ and t using the partial wave amplitudes of each Debye term (N, A, B) for $N \le 3$ as described in [1] in place of the full Aden–Kerker partial wave scattering amplitude, and then summing over partial waves as in Eqs. (1a,1b). Each of the previous ray theory identifications was verified by the Debye term partial wave sums. For the pulse and coated sphere parameters of this section, the analysis of the various Debye term partial wave sums showed that the terms (1, 2, 2) and (1, 4, 2) have first-order rainbows. The terms (2, 2, 3), (2, 4, 3), and (2, 6, 3) have second-order rainbows, and the terms (3, 2, 4), (3, 4, 2), (3, 4, 4), (3, 6, 4), and (3, 8, 4) have third-order rainbows that we denote by $\alpha\alpha\alpha$, $\alpha\beta\gamma$, $\alpha\alpha\beta$, $\alpha\beta\beta$, and $\beta\beta\beta$, respectively, where γ indicates the internal reflection R_n^{212} at the core/coating interface with incidence from the coating side. Glory scattering of nonaxial rays occurs for the terms (1, 2, 0), (1, 2, 2), (1, 4, 2), (2, 4, 1), (2, 6, 3), (3, 2, 4), (3, 4, 0), and (3, 4, 2). The term (3, 4, 4) has two different regions of forward glory scattering and will be discussed below. Surface wave glory scattering occurs in the terms (0, 2, 1), (2, 2, 3), (2, 4, 3), (3, 2, 4), (3, 4, 0), (3, 6, 2), (3, 6, 4), and (3, 8, 4). It is not surprising that so many ray paths participate in glory scattering since a large number of internal reflections can easily produce a large range of scattering angles that pass through 0° or 180° for nonaxial rays. As the number of internal

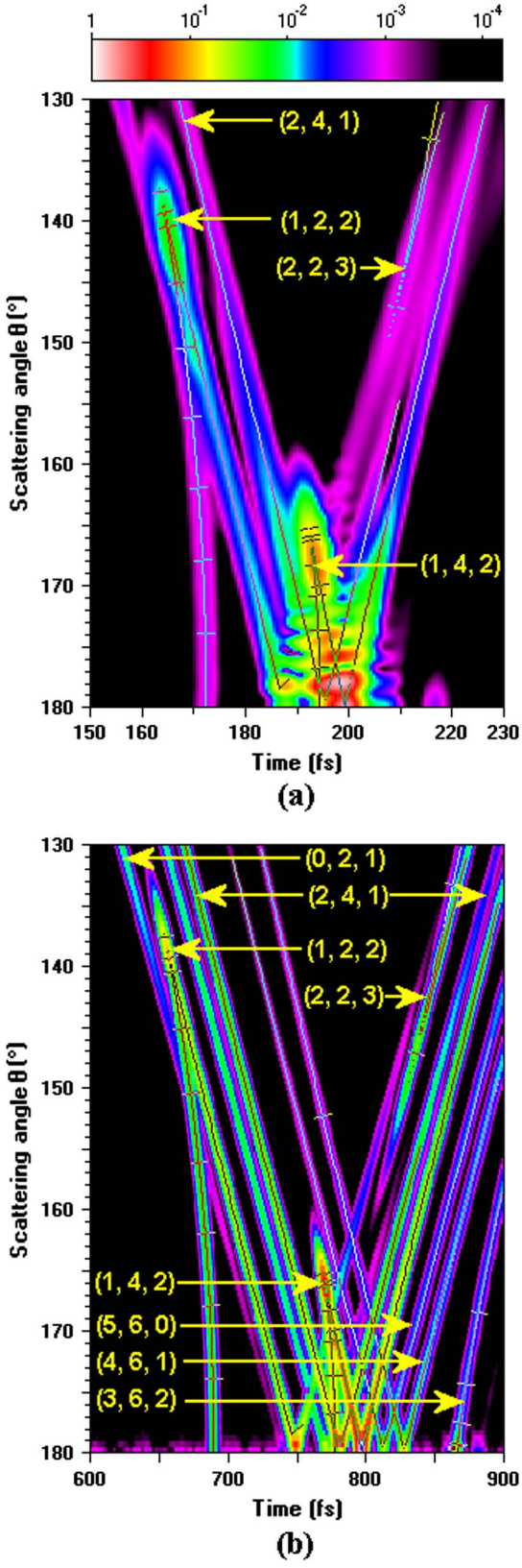

Fig. 2. (Color online) (a) Scattered intensity for the pulse and coated sphere parameters of Fig. 1 for 130° ≤ θ ≤ 180° and 150 fs ≤ t ≤ 230 fs in the region of the first-order rainbow. Various ray trajectories as a function of the incident ray impact parameter b are superimposed on the figure; (b) Scattered intensity for the pulse parameters of Fig. 1 but with $a_{12} = 30$ μm and $a_{23} = 40$ μm, which resolve additional structure of the scattered intensity in the vicinity of the first-order rainbow.

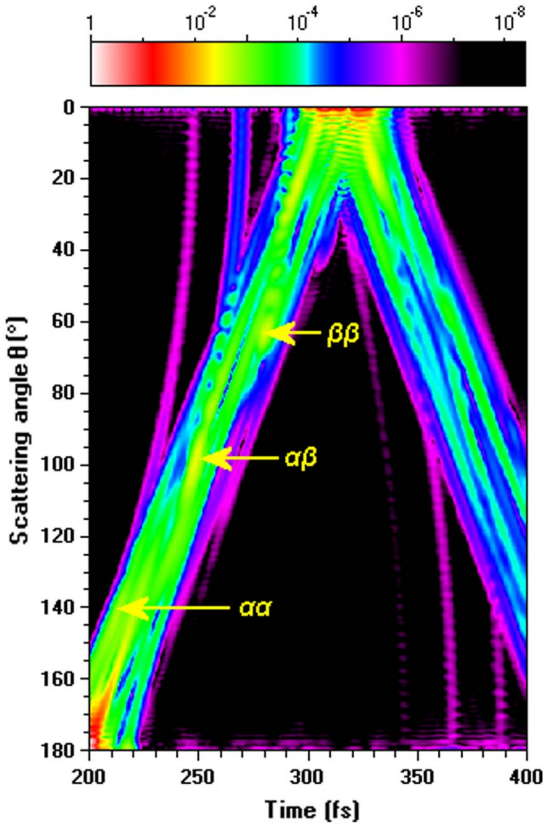

Fig. 3. (Color online) Scattered intensity for the pulse and coated sphere parameters of Fig. 1 for $0° \le \theta \le 180°$ and 200 fs $\le t \le$ 400 fs showing the behavior of the (2, 2, 3), (2, 4, 3), and (2, 6, 3) Debye terms and their $\alpha\alpha$, $\alpha\beta$, and $\beta\beta$ second-order rainbows.

reflections increases, progressively less energy remains in the pulse to be available for future transmissions or reflections, making high-N scattering intrinsically dimmer than low-N scattering. The fact that the wave focusing of either rainbow or glory scattering occurs in large number of high-N Debye terms partially compensates for this energy decrease and permits their visibility in Figs. 1–3.

As examples of some of the more interesting scattering features of an individual Debye term, the time domain graph of the twin first-order rainbows (1, 2, 2) and (1, 4, 2) is shown in Figs. 4(a) and 4(b), respectively. The Descartes rainbow scattering angles are $\theta \approx 139°$ and 166°, respectively. The complex ray [11] on the zero-ray side of the rainbow extends from the rainbow relative maximum to smaller scattering angles and smaller delay times. The contribution of rays in the two-ray supernumerary region [12], and its continuation into surface waves [13], extends from larger scattering angles, through the glory region, to smaller angles (which in this case are yet larger deflection angles) and larger delay times. Figure 4(c) shows the scattered intensity for the (3, 4, 2) Debye term, which has the repeated ray path in $\theta - t$ space of (1, 4, 2). The scattered intensity along the trajectory in (3, 4, 2) is weaker than for (1, 4, 2) due to the extra internal reflection factors at the core/coating interface.

Figure 5 is the time domain graph for scattering produced by the (2, 2, 3) Debye term. The most interesting feature of this figure is the complex ray glory of the $\alpha\alpha$ second-order rainbow at $t \approx 190$ fs. The Descartes rainbow angle for scattering by a homogeneous sphere depends on the sphere refractive index and the number of internal reflections. But since the rainbow angle for a coated sphere depends on the core and coating radii and refractive indices, as well as on the number of the three different types of internal reflections, one has a greater freedom in moving the rainbow angle around by changing various geometrical and physical parameters of the coated sphere, and thus generating effects such as the complex ray glory in Fig. 5. Figure 6 shows that the (3, 4, 4) Debye term produces the $\alpha\alpha\beta$ third-order rainbow at $b = 0.93$ and

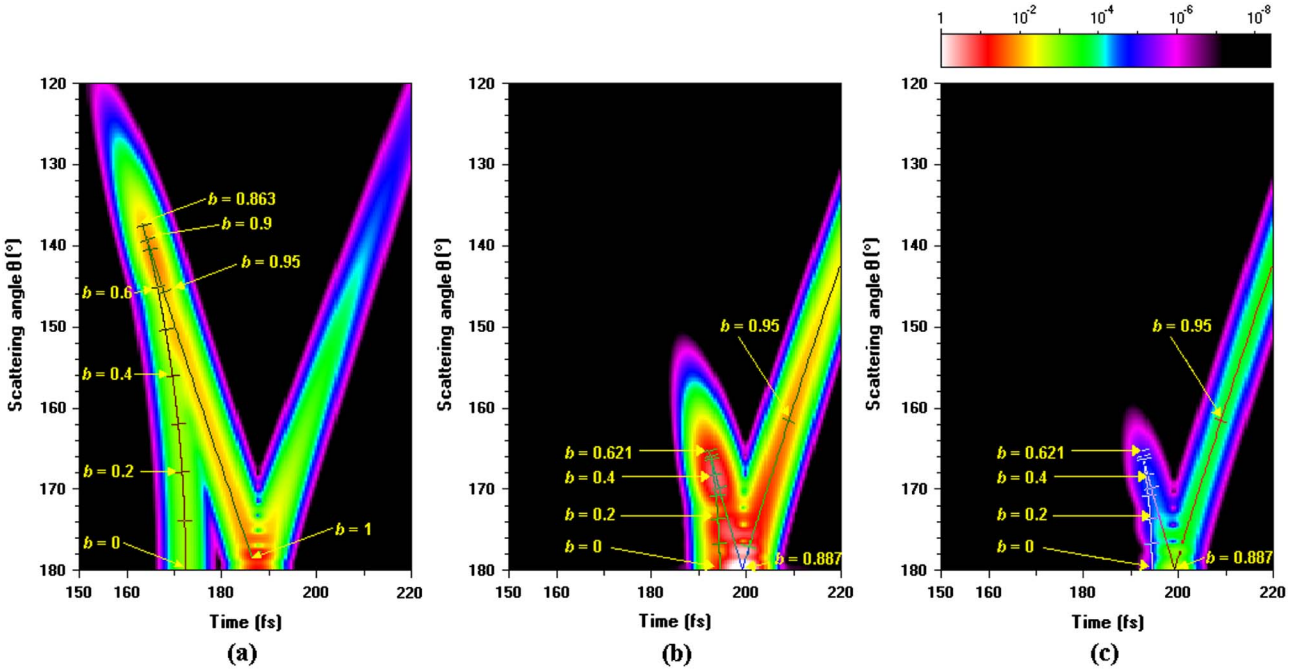

Fig. 4. (Color online) (a) Scattered intensity of the (1, 2, 2) Debye term for the pulse and coated sphere parameters of Fig. 1 showing the α first-order rainbow; (b) Scattered intensity of the (1, 4, 2) Debye term showing the β first-order rainbow; (c) Scattered intensity of the (3, 4, 2) Debye term, which has the same time domain trajectory as the (1, 4, 2) term.

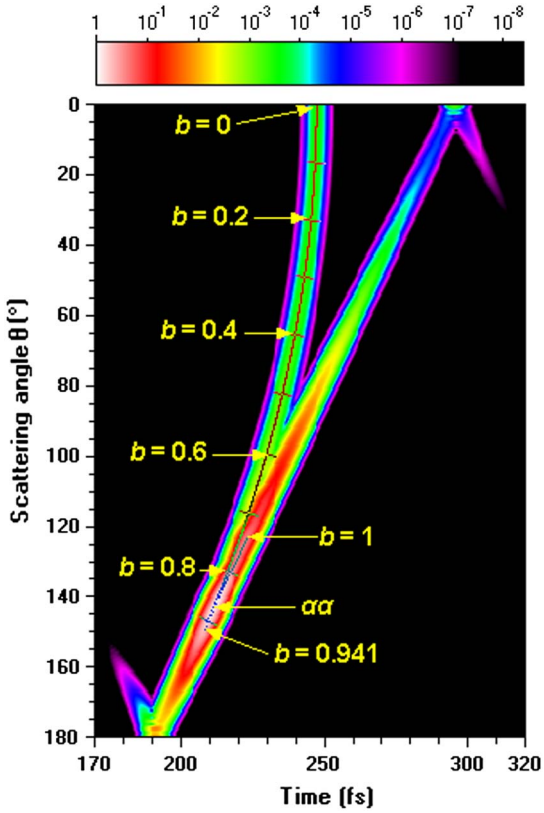

Fig. 5. (Color online) Scattered intensity of the (2, 2, 3) Debye term for the pulse and coated sphere parameters of Fig. 1 showing the glory at $\theta \to 180°$ and $t \approx 190$ fs caused by the complex ray of the $\alpha\alpha$ second-order rainbow.

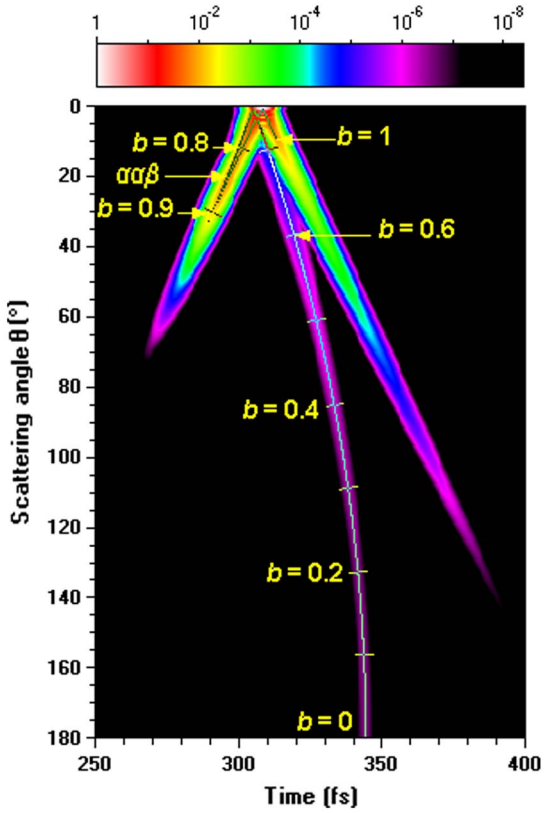

Fig. 6. (Color online) Scattered intensity of the (3, 4, 4) Debye term for the pulse and coated sphere parameters of Fig. 1 showing the $\alpha\alpha\beta$ third-order rainbow at $b = 0.93$ and $\theta \approx 20°$. As geometric rays with impact parameters on the coated sphere of $b = 0.7506$ and $b = 0.9968$ produce forward scattering ($\theta = 0°$), the (3, 4, 4) term also causes two forward glories (at $t \approx 305$ fs and $t \approx 308$ fs).

$\theta \approx 20°$. This rainbow consists of the three-fold degenerate contributions of Figs. 2(p), 2(q), and 2(r) of [1]. As geometric rays with impact parameters on the coated sphere of $b = 0.7506$ and $b = 0.9968$ result in forward scattering ($\theta = 0°$), Figure 6 also shows two forward glories. If the coated sphere parameters were slightly changed from the values considered here, the $\alpha\alpha\beta$ rainbow could be moved to $\theta = 0°$, producing a rainbow-enhanced forward glory [14]. The same effect occurs for the $p = 3$ rainbow-enhanced back scattering glory and the $p = 4$ rainbow-enhanced forward glory of a homogeneous sphere when the refractive index is $m = 1.180$ and 1.465, respectively. The two phenomena of Figs. 5 and 6 are thus different sections through the same overall rainbow-plus-glory morphology. As some geometrical or physical parameter is varied and the Descartes angle of a particular rainbow approaches either 0° or 180° and then passes through it, the complex ray glory evolves into a rainbow-enhanced glory, which then evolves into a pair of glories with a rainbow occurring at an intermediate impact parameter.

3. COATED SPHERE WITH A CORE OF VARIABLE RADIUS

Next we computed time domain scattering of a pulse with the same parameters in Section 2 by a coated sphere with $a_{23} = 10$ μm, but with the core radius increasing from $a_{12} = 0$ μm (i.e., a homogeneous sphere with refractive index $m = 1.3333$) to $a_{12} = 10$ μm (a homogeneous sphere with refractive index $m = 1.5$). Figures 7(a)–7(f) show this progression for $a_{12} = 0$, 2, 4, 6, 8, 10 μm for $0° \le \theta \le 180°$. In Fig. 7(a) the contribution of the $0 \le p \le 4$ Debye terms for a homogeneous sphere composed of coating material are clearly evident. The directly transmitted $p = 1$ rays have the critical angle $\theta_c = 82.82°$ and are continued to larger scattering angles and delay times by electromagnetic surface waves. The $p = 2$, 3, and 4 rainbows occur at the Descartes angles $\theta_D = 137.97°$, 129.04°, and 41.60°, respectively.

Figure 7(b) shows the time domain plot for $a_{12} = 2$ μm. The (0, 0, 0) external reflection term extends from $\theta = 180°$, $t = 0$ fs to $\theta = 0°$, $t \approx 80$ fs, with its distinctive inverted-V structure at $\theta \approx 0°$ produced by diffraction [9]. The nearly overlapping (1, 2, 0) and (0, 2, 1) terms occur for small θ at slightly larger t. The inverted-V structure of the (1, 2, 0) term has evolved from the $p = 1$ transmission term for a homogeneous sphere [7]. The left half of the inverted-V is due to scattered rays that have reflected off the core, and the right half is due to rays passing through the coating and missing the core. The core/coating surface waves of the (0, 2, 1) term for transmission through both the coating and core begin at $\theta = 62.40°$ and occur at slightly smaller delay times, have a steeper slope in the figure, and damp out more slowly as a function of θ than do the neighboring coating/exterior surface waves of (1, 2, 0), which begin at $\theta = 82.82°$, occur at slightly larger delay times, have a smaller slope in the figure, and damp out more rapidly. The (1, 2, 2) term weakly appears for $\theta \approx 180°$ and $t \approx 120$ fs and merges into the contribution of (0, 2, 1) surface waves. The rainbow region of the (3, 4, 0) term has evolved from the $p = 2$ term for a homogeneous sphere as described in [7], and occurs here for

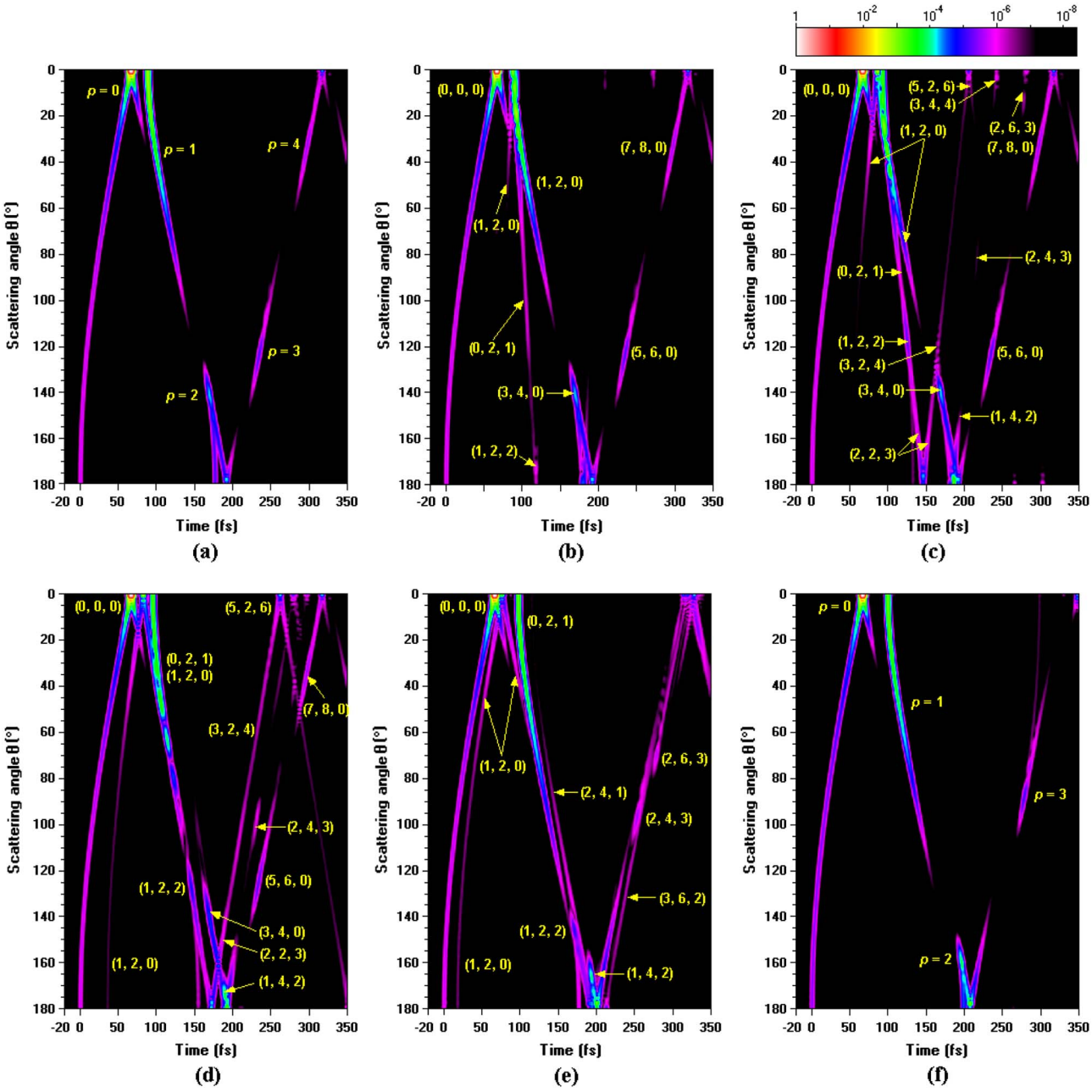

Fig. 7. (Color online) Scattered intensity as a function of θ and t for the incident pulse and coated sphere parameters of Fig. 1 except the core radius a_{12} is (a) 0, (b) 2, (c) 4, (d) 6, (e) 8, and (f) 10 μm. Figure 7(a) describes an uncoated sphere with $m = 1.3333$ and Fig. 7(f) describes an uncoated sphere with $m = 1.5$. See Media 1.

$130° \le \theta \le 180°$ and $t \approx 190$ fs. Yet longer delay times are dominated by the rainbow region of the (5, 6, 0) and (7, 8, 0) terms, which have evolved from the $p = 3$ and $p = 4$ terms of Fig. 7(a) as described in [7].

In Fig. 7(c) the core has grown to $a_{12} = 4$ μm. For $\theta \approx 0°$ and 70 fs $\le t \le$ 100 fs are the inverted-V structure of (0, 0, 0), followed by the inverted-V structure of (1, 2, 0), and finally the (0, 2, 1) term. Again the core/coating surface waves of (0, 2, 1) have a steeper slope than do the coating/exterior surface waves of (1, 2, 0). The contribution of the (0, 2, 1) surface waves merge into the complex ray of the α rainbow of (1, 2, 2). The (1, 2, 2) term also contributes to the V-shaped glory structure at $\theta = 180°$, $t \approx 145$ fs. This is followed for $\theta \approx 180°$, $t \approx 190$ fs by a portion of (1, 4, 2) superimposed on the rainbow region of (3, 4, 0). As before, yet larger delay times are dominated by the rainbow region of (5, 6, 0) and (7, 8, 0). Since the impact parameter of the $p = 3$ rainbow in Fig. 7(a) is $b = 0.95$, large impact parameter rays for (5, 6, 0) continue to participate in this second-order rainbow without being blocked by the relatively small core. The inverted-V structures at $\theta \approx 0°$ and $t \approx 205$, 242, 280 fs are the forward glories of the (5, 2, 6), (3, 4, 4), and (2, 6, 3) terms, respectively.

Figure 7(d) has $a_{12} = 6$ μm. For $\theta \approx 0°$ and 60 fs $\le t \le$ 100 fs, the (0, 0, 0) term is followed by (1, 2, 0) and finally (0, 2, 1). The (0, 2, 1) core/coating surface waves with steeper slope and the (1, 2, 0) coating/exterior surface waves with a smaller slope overlap and interfere for $40° \le \theta \le 100°$. For $\theta \approx 180°$ and larger delay times, the α

rainbow of the (1, 2, 2) term is followed by the rainbow region of (3, 4, 0) with a portion of (1, 4, 2) superimposed on it extending toward smaller θ and larger t. The extension of (1, 2, 2) starting at $\theta = 180°$, $t \approx 170$ fs merges into (3, 2, 4) and then into the forward glory region of (5, 2, 6) at $\theta = 0°$, $t \approx 260$ fs. At $\theta \approx 100°$, $t \approx 230$ fs is the $\alpha\beta$ second-order rainbow region of (2, 4, 3), and at $\theta \approx 130°$, $t \approx 230$ fs is the second-order rainbow region of (5, 6, 0) as it appeared in Figs. 7(a–c). Note the (7, 8, 0) glory, which has not changed since Fig. 7(a).

Figure 7(e) has $a_{12} = 8$ μm. The analysis of this figure is very similar to that of Fig. 1 where $a_{12} = 7.5$ μm. It should be noted that the $\alpha\beta$ and $\beta\beta$ second-order rainbows of (2, 4, 3) and (2, 6, 3) are quite visible, but the $\alpha\alpha$ second-order rainbow of (2, 2, 3) is too dim to be seen. Lastly, for $a_{12} = 10$ μm in Fig. 7(f), the structures of Fig. 7(e) merge into the various $0 \le p \le 3$ Debye terms of a homogeneous sphere composed of core material. The critical angle of the $p = 1$ transmitted rays is $\theta_c = 96.38°$, and the Descartes angle of the $p = 2$ and 3 rainbows are $\theta_D = 157.16°$ and 93.13°, respectively. The $p = 4$ rainbow is off the figure to the right. (See Media 1.)

Figures 8(a)–(8f) show the same progression of core radii, but in the restricted region $120° \le \theta \le 180°$ and 130 fs $\le t \le$ 220 fs, illustrating the evolution of the first-order rainbow of a coated sphere. Figure 8(a) shows the $p = 2$ rainbow of a homogeneous sphere of refractive index $m = 1.3333$. The Descartes rainbow angle is $\theta_D = 137.97°$ and the impact parameter of the rainbow ray is $b = 0.861$. Thus the core will have to grow to $a_{12} \approx 6.5$ μm before the rainbow ray is blocked by it and the rainbow is extinguished. The maximum rainbow intensity in Fig. 8(a) occurs at $\theta \approx 142°$. Given that the Fourier spectrum of the incident pulse has been integrated over in producing the maximum, this shift is in reasonable agreement with the Airy shift of the rainbow maximum due to finite particle size [15]. The theoretical shift is $\theta - \theta_D = 4.7°$ for $a = 10$ μm, $m = 1.3333$, and $\lambda = 0.65$ μm, the central wavelength of the Fourier spectrum.

Figure 8(b) has $a_{12} = 2$ μm. What had been the $p = 2$ rainbow in Fig. 8(a) is now contained in the (3, 4, 0) Debye term, which is also shown separately in Fig. 9 and will be discussed in detail later. As mentioned above, the Descartes rainbow angle is still $\theta_D = 137.97°$. The (3, 4, 0) core/coating surface waves pass through $\theta = 180°$ at $t \approx 180$ fs and continue with a steep slope to larger delay times as indicated by "A" in Fig. 8(b) with the (1, 4, 2) Debye term weakly superimposed on them. The (3, 4, 0) coating/exterior surface waves pass through $\theta = 180°$ at $t = 192$ fs and continue with a smaller slope to larger delay times as indicated by "B" in Fig. 8(b).

Figure 8(c) shows time domain scattering for $a_{12} = 4$ μm. The (3, 4, 0) rays that miss the core continue to participate in rainbow scattering with the Descartes angle $\theta_D = 137.97°$. This Debye term also dominates the back-scattering region for 170 fs $\le t \le$ 200 fs. As was the case in Fig. 8(b), the (3, 4, 0) core/coating surface waves plus a portion of (1, 4, 2) pass through $\theta = 180°$ at $t \approx 186$ fs and continue to smaller scattering angles and larger delay times with a steep slope, as indicated by "A" in Fig. 8(c), whereas the (3, 4, 0) coating/exterior surface waves start at $\theta \approx 166°$, $t \approx 182$ fs, pass through $\theta = 180°$ at $t \approx 192$ fs, and continue to smaller scattering angles and longer delay times with a smaller slope, as indicated by "B" in Fig. 8(c). Large impact parameter (1, 2, 2) rays and their continuation into surface waves produce the V-shaped structure extending from $t \approx 130$ fs to $t \approx 165$ fs. The (1, 2, 2) surface waves interfere with the complex ray of the (3, 4, 0) rainbow for $120° \le \theta \le 135°$ and $t \approx 165$ fs.

In Fig. 8(d) with $a_{12} = 6$ μm, an increasingly large fraction of the incident rays penetrate into the larger core giving more structure to (1, 2, 2) and (1, 4, 2), including the α and β first-order rainbows at $\theta \approx 127°$ and 175°, respectively. The contribution of the (1, 2, 2) core/coating surface waves is the V-shaped structure that starts at $\theta \approx 142°$, $t \approx 154$ fs, passes through $\theta = 180°$ at $t \approx 172$ fs, and extends to smaller scattering angles and longer delay times. The first ray that enters the coating and misses the core now has an impact parameter $b = 0.8$ that is still less than the impact parameter $b = 0.861$ of the first-order rainbow in the coating. As a result, the first order rainbow is still present with its maximum intensity at $\theta \approx 142°$. The (3, 4, 0) rays that miss the core by progressively larger distances extend out to $\theta \approx 166°$, $t \approx 182$ fs, at which point they generate (3, 4, 0) coating/exterior surface waves. What was originally the $p = 2$ rainbow for a homogeneous sphere in Fig. 8(a) has now evolved into three separate first-order rainbows at $\theta \approx 127°$, 142° and 175°. The original 142° component is in the process of being slowly extinguished as a_{12} increases, while the new α and β components at $\theta \approx 127°$ and 175° are becoming increasingly dominant.

When $a_{12} = 8$ μm in Fig. 8(e), all incident rays that enter the coating now penetrate into the core. This fully extinguishes all (3, 4, 0) scattering that formerly took place solely in the coating, including the former $p = 2$ rainbow. The (1, 2, 2) and (1, 4, 2) first-order rainbows have migrated to $\theta \approx 147°$ and 167°, and the α rainbow of (1, 2, 2) is now nestled between the (0, 2, 1) surface waves and the contribution of the (2, 4, 1) term. As a_{12} increases further, the (1, 2, 2) and (1, 4, 2) rainbows continue to approach each other, and in Fig. 8(f) with $a_{12} = 10$ μm they have now completely merged into the $p = 2$ rainbow of a homogeneous sphere composed of core material, having the Descartes angle $\theta_D = 157.16°$. The peak intensity at $\theta \approx 161°$ is again in reasonable agreement with the theoretical Airy shift of $\theta - \theta_D = 3.57°$. The details of this merging were studied in [4]. A similar transition occurs for the second-order rainbow, as is suggested in Figs. 3 and 7(c)–(7f). For a small core, the remnant of the $p = 3$ rainbow of a homogeneous sphere composed of coating material appears in the (5, 6, 0) term. For larger core radii, new $\alpha\alpha$, $\alpha\beta$ and $\beta\beta$ second-order rainbows form in the (2, 2, 3), (2, 4, 3), (2, 6, 3) terms while the original (5, 6, 0) rainbow slowly fades away. As $a_{12} \to a_{23}$, the three new components merge into the $p = 3$ rainbow of a homogeneous sphere composed of core material.

Electromagnetic surface waves are generated by grazing incidence at both the core/coating and coating/exterior interfaces. The scattered field of the core/coating surface wave was predicted in [1] to have the attenuation factor $\exp[-(m_2 k a_{12})^{1/3} 3^{1/2} X(\theta - \theta_c)/2^{4/3}]$, where θ_c is the critical scattering angle and $-X$ is the first zero of the Airy function, with $X \approx 2.3381$. This result is analogous to the attenuation factor $\exp[-(m_3 k a_{23})^{1/3} 3^{1/2} X(\theta - \theta_c)/2^{4/3}]$ of the scattered field of the coating/exterior surface wave [16,17]. Time domain scattering of the (3, 4, 0) Debye term is shown in Figs. 9(a–c) for $a_{23} = 10$ μm and $a_{12} = 2.5$, 5 and 7.5 μm, respectively. For incident impact parameters in the range $0 \le b \le 0.333$, the (3, 4, 0) rays in Fig. 9(a) produce a deflection angle that increases from $\theta = -180°$ for axial incidence to $\theta = +161.0°$

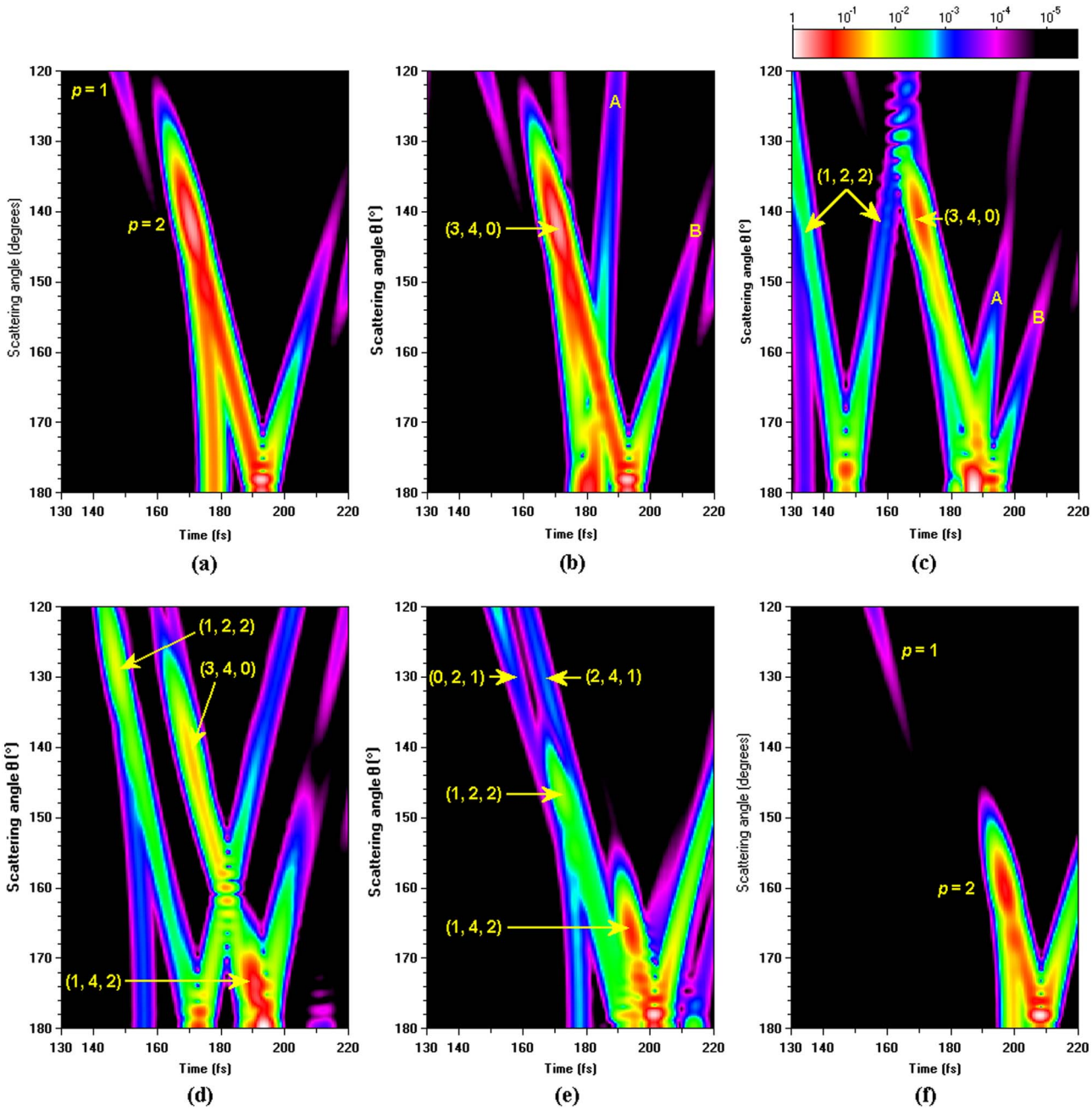

Fig. 8. (Color online) Scattered intensity as in Fig. 7 but for $120° \le \theta \le 180°$ and 130 fs $\le t \le$ 220 fs in the vicinity of the first-order rainbow showing its evolution for core radius a_{12} of (a) 0; (b) 2; (c) 4; (d) 6; (e) 8; and (f) 10 μm. The features marked "A" are caused by core/coating surface waves, whereas the features marked "B" are caused by coating/exterior surface waves.

with infinite slope there, for grazing incidence on the core and the generation of core/coating surface waves. For $0.333 < b \le 1$, the partial waves corresponding to these incident rays miss the core by a progressively larger distance, but still interact with it via tunneling reflection with the amplitude $R_n^{212} \to 1$ [16]. In this impact parameter interval, the ray deflection angle decreases from $\theta = +161.0°$ to the Descartes rainbow angle of $\theta_D = 137.97°$, and then increases back to $\theta = 165.6°$ for grazing incidence on the coating and the generation of coating/exterior surface waves. This is exactly what happened for $p = 2$ scattering by a homogeneous sphere with $m = 1.3333$. Although Fig. 9(a) shows no indication of a relative maximum of this Debye term at $\theta = +161.0°$, it would be of interest to determine whether this evolves into an additional first-order rainbow [18], in the sense of producing partial focusing of the scattered light, if the sharp core/coating interface at $a_{12} = 2.5$ μm were replaced by a narrow radial interval of decreasing refractive index.

The (3, 4, 0) Debye term simultaneously exhibits two different types of surface waves. In Fig. 9(a), the core/coating surface waves (marked as "A") pass through $\theta = 180°$ at $t \approx$ 180 fs and extend to smaller scattering angles and larger time delays with a steep slope, while the coating/exterior surface waves (marked as "B") pass through $\theta = 180°$ at $t \approx 192$ fs and also extend to smaller scattering angles and larger time delays, but with a smaller slope.

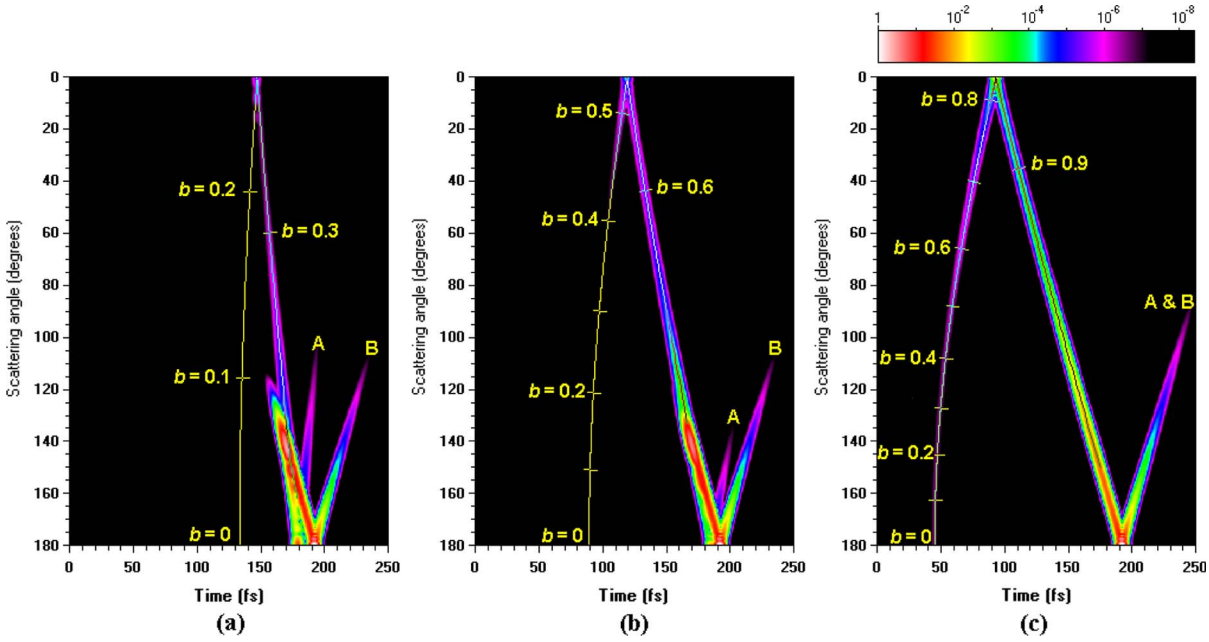

Fig. 9. (Color online) Scattered intensity of the (3, 4, 0) Debye term as a function of θ and t for the incident pulse and coated sphere parameters of Fig. 1, except that the core radius a_{12} is (a) 2.5, (b) 5 and (c) 7.5 μm, showing the evolution of the core/coating surface waves (marked as "A") and coating/exterior surface waves (marked as "B") of this Debye term. In (c) the two types of surface waves coalesce. The (3, 4, 0) ray trajectory as a function of the incident ray impact parameter b is superimposed on the figures.

In Fig. 9(b) for $a_{12} = 5$ μm, the coating/exterior surface wave has not changed from Fig. 9(a) since a_{23} has been held constant. But the slope of the core/coating surface wave progressively decreases and the two surface wave contributions start to merge. For $a_{12} = 7.5$ μm in Fig. 9(c), the incident rays that graze the coating/exterior interface and are transmitted into the coating also graze the core/coating interface. As a result, the same incident rays create both sets of surface waves, and the merging of the two surface wave contributions becomes complete.

4. CONCLUSION

The (N, A, B) parameterization of the Debye series terms in [1] proves to be very useful for interpreting time domain scattering of a plane wave by a coated sphere. The great virtue of time domain scattering is that it separates into different delay times all the different scattering mechanisms that contribute at the same scattering angle. Many (N, A, B) Debye series terms were easily identified in different regions of $\theta - t$ space in the time domain graph, both on the basis of ray tracing assignments and on summing the appropriate partial wave amplitudes. Using the combined power of time domain scattering methods and the (N, A, B) organization of the Debye series, the wonderful richness of the structure to be uncovered in scattering by a coated sphere is clearly evident.

If a homogeneous sphere were to continuously change its refractive index relative to its surroundings, perhaps by placing a solid sphere in a liquid of controlled temperature [14], the first-order rainbow would continuously and smoothly evolve from one angle to another. But if the transition were to occur by either the growth of a seed particle within a sphere or the growth of a coating around a core, the first-order rainbow would undergo a more complicated and delicate evolution. Before the old rainbow fades out, a number of new rainbows start to form, which then migrate and eventually merge into the final rainbow. Again the power of time domain scattering methods coupled with the (N, A, B) organization of the coated sphere Debye series illustrate this evolution in a remarkably clear way.

REFERENCES

1. J. A. Lock and P. Laven, "Understanding light scattering by a coated sphere. Part 1: Theoretical considerations," J. Opt. Soc. Am. A **29**, 1489–1497 (2012).
2. A. L. Aden and M. Kerker, "Scattering of electromagnetic waves from two concentric spheres," J. Appl. Phys. **22**, 1242–1246 (1951).
3. K. A. Fuller, "Scattering of light by coated spheres," Opt. Lett. **18**, 257–259 (1993).
4. J. A. Lock, J. M. Jamison, and C.-Y. Lin, "Rainbow scattering by a coated sphere," Appl. Opt. **33**, 4677–4690 (1994).
5. H. C. van de Hulst, "The localization principle," in *Light Scattering by Small Particles* (Dover, 1981), pp. 208–209.
6. P. Laven, "Separating diffraction from scattering: the million dollar challenge," J. Nanophoton. **4**, 041593 (2010).
7. P. Laven, "Time domain analysis of scattering by a water droplet," Appl. Opt. **50**, F29–F38 (2011).
8. J. A. Lock and P. Laven, "Mie scattering in the time domain. Part 1. The role of surface waves," J. Opt. Soc. Am. A **28**, 1086–1095 (2011).
9. J. A. Lock and P. Laven, "Mie scattering in the time domain. Part II. The role of diffraction," J. Opt. Soc. Am. A **28**, 1096–1106 (2011).
10. H. C. van de Hulst, "Amplitude functions," in *Light Scattering by Small Particles* (Dover, 1981), pp. 124–126.
11. H. M. Nussenzveig, "Complex angular momentum theory of the rainbow and the glory," J. Opt. Soc. Am. **69**, 1068–1079 (1979).
12. J. D. Walker, "Multiple rainbows from single drops of water and other liquids," Am. J. Phys. **44**, 421–433 (1976).
13. H. M. Nussenzveig, "High-frequency scattering by a transparent sphere. II. Theory of the rainbow and the glory," J. Math. Phys. **10**, 125–176 (1969).

14. D. S. Langley and M. J. Morrell, "Rainbow-enhanced forward and backward glory scattering," Appl. Opt. **30**, 3459–3467 (1991).
15. A. B. Fraser, "Why can the supernumerary bows be seen in a rain shower?" J. Opt. Soc. Am. **73**, 1626–1628 (1983).
16. H. M. Nussenzveig, "High-frequency scattering by a transparent sphere. I. Direct reflection and transmission," J. Math. Phys. **10**, 82–124 (1969).
17. V. Khare, "Short-wavelength scattering of electromagnetic waves by a homogeneous dielectric sphere," Ph.D. dissertation (University of Rochester, 1975).
18. J. A. Adam and P. Laven, "Rainbows from inhomogeneous transparent spheres: a ray-theoretic approach," Appl. Opt. **46**, 922–929 (2007).